ACS Catalysis

Research Article

pubs.acs.org/acscatalysis

Importance of Particle Size and Distribution in Achieving High-Activity, High-Stability Oxygen Reduction Catalysts

Ying Liu,[†,‡] Lichun Zhang,[§] Brian G. Willis,[†] and W. E. Mustain*,[†,‡,§]

[†]Department of Chemical & Biomolecular Engineering, University of Connecticut Storrs, Connecticut 06269-3222, United States

[‡]Center for Clean Energy Engineering, University of Connecticut, Storrs, Connecticut 06269-5233, United States

[§]Institute of Materials Science, University of Connecticut, Storrs, Connecticut 06269-3136, United States

Supporting Information

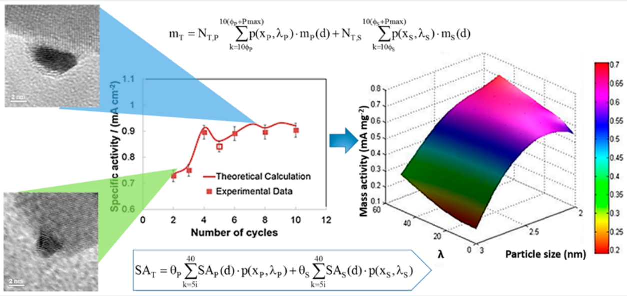

ABSTRACT: Strongly interacting catalyst supports can influence the nucleation, growth, dispersion, and shape of supported nanoparticles that impact catalytic activity and stability. However, there is little understanding of the limitations of support interactions, and the ability to quantitatively relate particle growth and loading to activity and stability is lacking. Here, we report a statistical framework to quantify the growth of a binary distribution of Pt nanoparticles on tin-doped indium oxide and predict mass and specific activity for the oxygen reduction reaction in acid media with increased Pt loading. Our results reveal that the growth mechanism for Pt on the oxide is directly related to its exceptional electrochemical activity and provide new insight into the relationship between nanoparticle size distribution and activity trends. We also show that catalyst degradation mechanisms can be controlled or altogether eliminated through strong metal−support interactions. The results of this work provide insights into how catalyst preparation influences material and chemical properties and how to develop design goals for next generation catalysts.

KEYWORDS: *particle size, catalyst, oxygen reduction reaction, fuel cells, statistical model*

1. INTRODUCTION

Pt-based electrocatalysts remain the most efficient materials at both the anode and cathode of the proton exchange membrane fuel cell (PEMFC).[1,2] Unfortunately, widespread commercialization of PEMFCs remains inhibited by a combination of slow kinetics and the poor stability of carbon-supported catalysts, particularly at the oxygen electrode. Controlling the morphology of Pt nanostructures (size, facet, etc.) can provide a powerful method to enhance the specific and mass activities of Pt.[3] This is particularly true for the oxygen reduction reaction (ORR) at the PEMFC cathode, where the activity is extremely structure sensitive. The low-index crystallographic facets of Pt show increased activities for the ORR on the order of Pt(100) ≪ Pt(111) < Pt(110), which likely results from the structure-sensitive inhibiting effects of OH_{ad} species on Pt facets that block active sites for O_2 adsorption and retard ORR kinetics.[4−6] However, it is difficult to prepare high-surface-area Pt nanoparticles with the desired facets because Pt nanoparticles <5 nm in size tend to exist as truncated octahedrons covered by a mix of {100} and {111} facets in an effort to minimize free energy.[7,8]

Precisely controlled growth of metal nanostructures with the desired orientation and alignment on substrates has become increasingly important in areas of plasmonics,[9] nanoelectronics,[10] and quantum devices[11] because it enables carefully tailored electronic, optical, magnetic, and catalytic properties. The most commonly used substrates for these applications are planar thin films, which limits application in certain areas, including supported catalysis. Although a few morphology-controlled particle catalysts have been achieved, they typically involve core−shell structures in which contiguous monolayer films of catalyst are deposited onto metallic nanoparticles.[12] Although more widely used support materials, including oxides, carbides, and nitrides, may strongly affect nucleation, growth, and morphology of catalytic nanoparticles, these effects have not been broadly investigated.

In our previous work, we found that Sn-doped indium oxide (ITO) interacts with Pt so strongly that Pt nanoparticles grow with continuous lattice fringes from dislocations in the ITO. This strong interaction leads to the growth of Pt nanoparticles with preferential {111} faceting with high ORR activity and excellent stability that already exceed the 2017 DOE targets for commercial fuel cells.[13] This suggests that investigations of Pt growth on strongly interacting supports are promising directions for next generation ORR electrocatalysts; however, much work remains to optimize their performance and realize property improvements in related catalytic systems. One key issue is that with such strong underlying substrate effects, it is

Received: October 9, 2014
Revised: December 30, 2014
Published: January 28, 2015

DOI: 10.1021/cs501556j
ACS Catal. 2015, 5, 1560−1567

unclear how the Pt morphology will scale to high loadings typical of PEMFCs and how this behavior compares with that of typical Pt/C catalysts.

In this work, we explore the growth of platinum nanoparticles by galvanic displacement on ITO supports as the Pt loading is increased. The shape, dispersion, and particle size provide insight into the electrochemical properties of Pt/ITO, including mass and specific ORR activity and stability, with increased loading. The methodology developed in this study can be expanded to other catalyst−support systems and may provide new insight into how nanoparticle growth impacts material properties and why different synthesis methods produce catalysts with different activities despite similar loadings. There is also potential to use the method to develop specifications for enhanced catalyst properties, including optimal loading and particle size distributions.

2. EXPERIMENTAL SECTION

2.1. Materials and Methods. The synthesis of the ITO supports was detailed in our previous work.[13] In short, indium acetylacetonate (In(acac)$_3$) and tin bis-acetylacetonate dichloride (Sn(acac)$_2$Cl$_2$) were dissolved in oleylamine and heated at 250 °C in air for 3 h, then ethanol was added to precipitate amorphous ITO that was dried at 80 °C under vacuum for 24 h and crystallized by calcining at 500 °C in air for 3 h. The Pt loading on the ITO was carefully controlled by Cu deposition, followed by galvanic displacement with Pt. The Pt mass loading was varied between 16% and 47%. Details for the Cu deposition and galvanic displacement can be found in the Supporting Information. Cu layers were deposited on the ITO surface by cycling the electrode potential 2, 4, 6, 8, and 10 times.

2.2. Electrochemical Experiments. Electrochemical experiments were conducted in a custom-built three-electrode electrochemical cell with a Luggin capillary (Adams & Chittenden Scientific Glass). All studies were carried out in 0.1 M HClO$_4$ at room temperature using an Autolab PGSTAT302N potentiostat with a platinum flag as the counter electrode and reversible hydrogen electrode (RHE) as the reference electrode. Results are reported in this paper with reference to RHE. The prepared Pt/ITO catalysts were fixed onto a 5 mm glassy carbon disk electrode (GCE) by dropping 20 μL of diluted DE-520 Nafion solution (1/100, 5 wt %, DuPont). To evaluate the oxygen reduction reaction (ORR), the electrolyte was bubbled with O$_2$ for 1 h and at least 5 cyclic voltammograms (CVs) were run at 50 mV/s to condition the electrode before the data were recorded. For the rotating disk electrode (RDE) measurements, the working electrode was scanned cathodically at a rate of 10 mV/s with varying rotating speeds from 400 to 2500 rpm. Detailed information is available in the Supporting Information file.

3. RESULTS AND DISCUSSION

3.1. Pt Nucleation and Growth. The Pt loading on ITO was systematically increased from 16 to 46 wt % through controlled Cu electrodeposition cycles, followed by spontaneous galvanic displacement by Pt. Pt/ITO catalysts were prepared with 2, 4, 6, 8, and 10 deposition cycles. Cyclic voltammograms for the Cu deposition cycles, experimental details, and loading calculations are provided in the Supporting Information. Pt particle size distribution and representative high-resolution transmission electron microscopy (HRTEM) images of the resulting Pt/ITO electrocatalysts are shown in Figure 1. The Pt/ITO catalysts with low Pt loadings, 2 and 4 deposition cycles, showed a single particle morphology. For a vast majority of the catalysts, the Pt nanoparticles were completely isolated from each other with only one nanoparticle per ITO facet. The insets of Figure 1a,b show HRTEM images of a single Pt nanoparticle, which show the intimate attachment of the Pt to the ITO surfaces. The Pt nanoparticles were dominated by {111} facets and revealed highly ordered continuous lattice fringes from ITO through the Pt nanoparticles, identical to our previous work with 3 deposition cycles of Pt/ITO.[13] A HRTEM image for 3 deposition cycles of Pt/ITO that very clearly shows Pt growth on ITO with

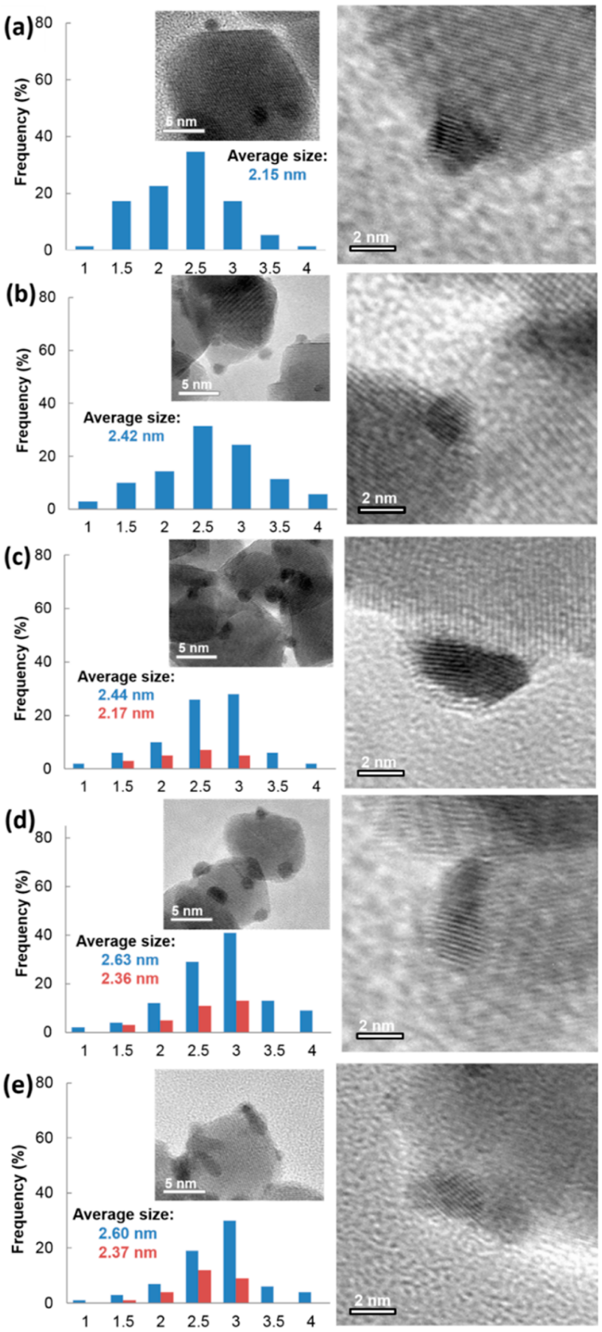

Figure 1. Pt particle size distribution and associated HRTEM images for Pt/ITO electrocatalysts with (a) 2, (b) 4, (c) 6, (d) 8, and (e) 10 deposition cycles. Blue, primary particles; red, secondary particles.

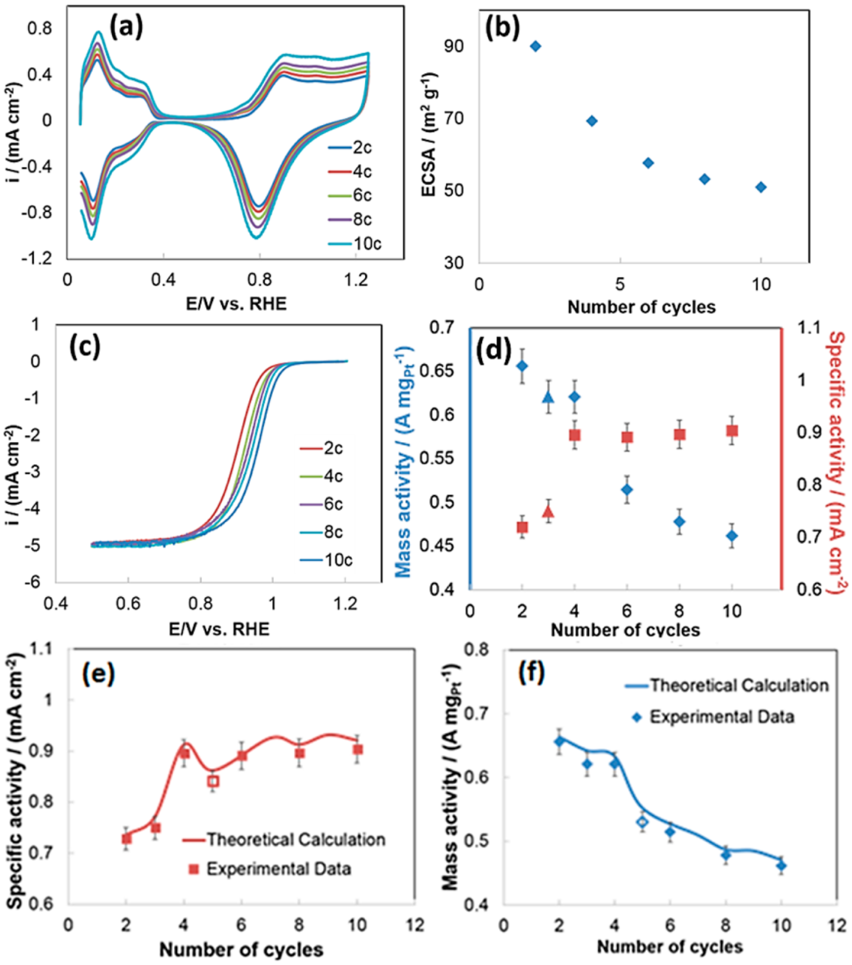

Figure 2. (a) Cyclic voltammograms of Pt/ITO prepared with different cycle numbers of Pt deposition in a N_2-saturated 0.1 M $HClO_4$ solution recorded at room temperature. Sweep rate, 50 mV/s. (b) Specific ECSA as a function of the number of Pt deposition cycles. (c) Polarization curves of Pt/ITO in O_2-saturated 0.1 M $HClO_4$ solution. Sweep rate: 10 mV/s. (d) Specific activity (red) and mass activity (blue) of Pt/ITO for oxygen reduction reaction at 0.9 V. The specific activity and mass activity of Pt/ITO with 3 DCs from previous study are also included for comparison; Theoretical fitting of the (e) specific activity and (f) mass activity of Pt/ITO for 2−10 deposition cycles. The open data points in e and f represent experimental data for five-deposition-cycle Pt/ITO.

continuous lattice fringes is shown in Figure S2. These Pt/ITO arrangements are very different from Pt/C and indicate that ITO substrates strongly affect Pt deposition, growth, and morphology.

At 6 deposition cycles (37 wt % Pt), a distribution of two types of particles emerges. Though well isolated nanoparticles still dominated the surface, Pt aggregates started to appear, as shown in Figure 1c. These aggregates consist almost exclusively of two adjoining Pt particles with different faceting. The larger primary particles maintain the preferential faceting observed for 2−4 deposition cycles. The secondary particles show different lattice fringes not aligned to the ITO substrate, and distinct from the primary particles. Because of their orientation relative to the primary particles, regardless of the total Pt loading, it appears that the secondary particles are nucleated from the primary particles as opposed to the ITO support. The sizes of primary particles were always <4 nm, and the secondary particle size never exceeded 3 nm. As the number of deposition cycles increased to 8 (Figure 1d) and 10 (Figure 1e), the emergence and growth of secondary particles was even more apparent as an increased number of two-particle agglomerates and three-particle agglomerates appeared.

3.2. Electrochemical Behavior of Pt/ITO Catalysts with Increased Loading. As the Pt loading increases, the number of surface atoms also increases. This is reflected by the electrochemically active surface area (ECSA) determined from the H adsorption features of CVs collected in N_2-saturated 0.1 M $HClO_4$ solution at 20 °C (Figure 2a). Although the absolute value of the Pt ECSA increases with loading, the specific ECSA shows an inverse relationship (Figure 2b). The specific ECSA decreases with higher Pt loadings from 90.1 to 52.3 $m^2\ g_{Pt}^{-1}$ as the ratio of surface to bulk atoms decreases. As the number of surface atoms increases, the ORR current between 0.8 and 1.0 V increases, shown by polarization curves in Figure 2c for 2, 4, 6, 8, and 10 deposition cycles. The ORR activity was determined from the mass transport corrected current at 0.9 V measured in O_2-saturated 0.1 M $HClO_4$ electrolyte using a thin-film RDE at 1600 rpm. The mass and specific activities at 0.9 V of the Pt/ITO catalysts are shown in Figure 2d.

It is well established for Pt nanoparticles supported on carbon that the specific activity increases rapidly as the particle grows to around 2.0 nm and then increases linearly as particle size further increases to 10 nm (the activity of nanoparticles with diameters greater than around 10 nm approach that of extended surfaces[14]); however, the trend for Pt/ITO is different. The specific activity increases sharply from ~0.728 to ~0.896 mA cm^{-2} going from 2 to 4 deposition cycles and then is nearly constant with further increases in catalyst loading. As discussed earlier, the high specific activity of Pt/ITO is at least partially due to the modified nanoparticle shape compared with Pt black and Pt/C as a result of the preferential exposure of high activity Pt {111} facets.[13] As long as the preferential faceting could be maintained with increased particle size, the specific activity would be expected to also increase because of a smaller percentage of edge and step sites that adsorb oxygen intermediates too strongly. However, TEM images show that secondary particles start to form at 6 deposition cycles, and the preferential {111} faceting is not observed on these particles. It is the counteracting effects of the high activity primary particles and the emergence of lower activity secondary particles that leads to the saturation of the specific activity at ~0.9 mA/cm$^2_{\mathrm{Pt}}$, which is confirmed by the particle distribution model discussed later.

Electrochemical Stability. Another catalyst property in which size, shape, distribution, and support interactions play a key role is electrochemical stability. Typically, the stability of Pt/C catalysts is negatively influenced by the support. Both carbon corrosion and weak support interactions for Pt/C act to reduce the ECSA and ORR mass activity rapidly with time.[15,16] Simply looking at the Pourbaix diagram,[17] it would be expected that the host structure, In_2O_3, would also be unstable in the ORR reacting environment; however, a closer look at the text in the Pourbaix Atlas reveals that at low pH and elevated potential, the surface remains passivated with metastable In_2O_3. This suggests that the indium oxide support will have favorable stability, which has been borne out in recent experiments.[13,18] It is well-known that small nanoparticles are more susceptible to activity loss than larger ones because of their high surface energy and zero-dimensional structural features.[19] However, for primary Pt nanoparticles supported on ITO, the structure and metal−support interactions are significantly different from both Pt/C and secondary particles on ITO.

The ECSA and ORR stability of Pt/ITO electrocatalysts were studied by cycling the potential between 0.0 and 1.4 V at 10 mV/s 1000 times (Supporting Information, Figures S3−S5). For the 2 and 4 deposition cycle catalysts with only primary particles, there was no recordable loss of Pt ECSA and no discernible physical degradation of the samples (Figure S4). However, increasing ECSA loss was observed for the catalysts with higher Pt loadings: 3%, 5%, and 9% loss were measured for 6, 8, and 10 deposition cycles, respectively. Regarding the ORR activity, the 2 and 4 deposition cycle catalysts showed only a 3 mV shift in the half-wave potential over the cycling period, which is markedly improved over commercial 20 wt % Pt/C catalysts that show 20 mV loss during the same treatment (Figure S6). The 6, 8, and 10 deposition cycle catalysts show 7, 10, and 12 mV degradation in the half-wave potential, respectively (Figure S3b). The accelerated ECSA loss and significant shift in the ORR half-wave potential were tied directly to the appearance of the secondary particles seen in Figures 1c−e.

When combined, the results of HRTEM studies and stability measurements suggest two key advantages for Pt/ITO compared with the state-of-the-art Pt/C electrocatalysts. First, these results show that the ITO support is intrinsically stable in the ORR regime and would be stable during startup/shutdown in a PEMFC, eliminating one of the key degradation mechanisms of Pt/C catalysts. Second, at low Pt loadings, where the primary particles are isolated from one another and attached strongly to the support, there is no Pt growth or agglomeration, implying that the Ostwald ripening mechanism is not active.

The other primary degradation route for supported Pt catalysts is Pt dissolution, which is facilitated by the formation of surface oxides.[16] The most common method to evaluate the dissolution resistance for supported catalysts is to rapidly cycle the catalyst between a low oxidation state (~0.6 V) and a highly oxidized state (~0.9 V). In this work, the Pt catalyst was load-cycled to test the Pt dissolution stability (Figure S5a). A 3 deposition cycle Pt/ITO sample was exposed to 5000 load cycles in an O_2-saturated 0.1 M $HClO_4$ solution at 60 °C. The first and 5000th cycle are shown in Figure S5b. Again, the Pt/ITO showed excellent stability. The CV responses changed negligibly after 5000 load cycles, which shows that Pt/ITO primary particles have excellent stability, enabled by their preferred shape and robust attachment to the support.

3.3. Impact of Particle Size Distribution on Pt Activity.

High-resolution TEM images are one of the most attractive platforms to accurately determine the size distribution of supported Pt particles. The measurements have good accuracy, ~0.2−0.5 nm is common, and the relative uncertainty can be low because it is dictated by the number of particles in the processed images (typically dozens to hundreds). Despite this capability, the most common utilization of this information in the literature is to present a numerically average particle size and perhaps the standard deviation, assuming a normal distribution. Observed catalytic behavior is often ascribed to particles with the measured average size.

There are several limitations of this approach, including the fact that nucleation and growth mechanisms are strongly dependent on the synthesis method,[7,20,21] and the particle size distribution of catalysts prepared by different methods may not be the same, even if the average particle sizes are similar. Moreover, the particle size distribution is often not Gaussian.[22] These concerns are especially important for structure sensitive reactions such as the ORR.[23] Lumping catalytic performance into a single size descriptor ignores critical details of the measured activity. Currently, there is a lack of understanding as to how particle size distributions contribute to PEMFC catalyst performance.

Here, we introduce a modified Poisson distribution function to capture the particle size distributions for both primary and secondary particles of our Pt/ITO electrocatalysts. The particle size distribution has two parameters, ϕ and λ, that determine the inflection point of the cumulative distribution function and the distribution width, respectively. The probability distribution and cumulative distribution function are given as eqs 1 and 2,

$$\mathrm{p}(x,\lambda) = \frac{\lambda^{x}\exp[-\lambda]}{x!},\quad x = 10\phi, 10\phi+1, 10\phi+2, ..., 10(\phi+P_{\max}) \tag{1}$$

$$\mathrm{CDF}(x,\lambda,\phi) = \sum_{k=10\phi}^{10(\varphi+P_{\max})} \frac{\lambda^{(k-10\phi)}\exp[-\lambda]}{(k-10\phi)!} \tag{2}$$

where x is an integer counter of possible particle sizes, $p(x,\lambda)$ is the probability of state x, and $P_{\max}$ is the largest observed particle size (4 nm for primary particles, 3 nm for secondary particles). For each catalyst preparation with different numbers of deposition cycles, HRTEM images were analyzed to

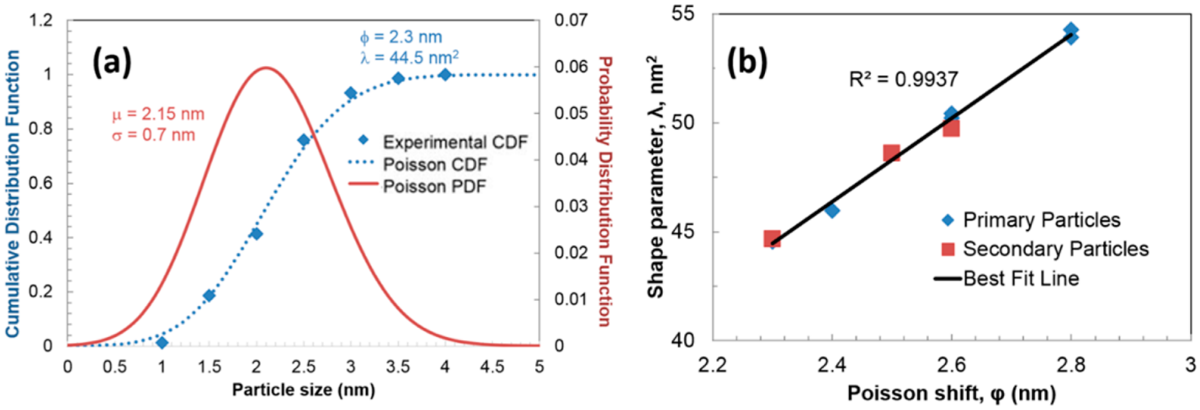

Figure 3. (a) The experimental CDF, Poisson CDF, and probability distribution function for 2 DC Pt/ITO. (b) The linear relationship between the shape parameter and Poisson shift for primary and secondary Pt particles for Pt/ITO for all cycle depositions.

determine the cumulative distribution and determine the parameters λ and ϕ. Additional details of the particle size distribution, including experimental data, averages, and standard deviations, are given in the Supporting Information.

An example of the experimental data and fit to the probability distribution for the 2 deposition cycle Pt/ITO sample is shown in Figure 3a. The R^2 value was 0.996, and the residuals appeared random, suggesting no systematic error. The modified Poisson distribution adequately captured the size distributions for all samples with different numbers of deposition cycles, yielding ϕ and λ parameters for each case. For the higher loadings, separate distributions were fit for both primary and secondary particles. The data and plots for the cumulative distribution functions, probability distributions, average particle sizes, and standard deviations for all samples are given in Figure S7 and summarized in Table S2. The effective R^2 value for all cases was >0.97.

The analysis shows that average primary particle size increased with Pt loading from 2.15 to 2.63 nm. The larger particles, observed at 6 or more deposition cycles, were accompanied by the emergence of secondary particles, whose average sizes increased from 2.17 to 2.37 nm with increased loading. Distributions of both primary and secondary particles broadened with an increase in Pt loading. The primary particle λ values increased from 44.5 to 53.9, and the secondary particles increased from 44.7 to 49.7. Though the trends for λ and ϕ are not surprising, an interesting observation is that λ and ϕ are linearly related. In addition, the primary and secondary particles share the same slopes for λ vs ϕ, despite their structural differences (Figure 3b).

The combined knowledge of Pt loadings and ratios of primary to secondary particles with the probability distributions were used to determine the number of primary and secondary particles, total number of surface atoms, and the ratio of primary and secondary surface atoms. For example, the total mass of Pt can be expressed as a summation of primary and secondary particles, as shown in eq 3.

$$m_T = N_{T,P} \sum_{k=10\phi_P}^{10(\phi_P+P_{\max})} p(x_P, \lambda_P)\cdot m_P(d) + N_{T,S} \sum_{k=10\phi_S}^{10(\phi_S+P_{\max})} p(x_S, \lambda_S)\cdot m_S(d) \quad (3)$$

In eq 3, $N_{T,P}$ and $N_{T,S}$ represent the total numbers of primary and secondary particles, respectively. The factors $p(x_P,\lambda_P)$ and $p(x_S,\lambda_S)$ represent the probability distributions of primary and secondary particles, respectively, and $m_p(d)$ and $m_s(d)$ are the masses of individual particles of diameter $d = k/10$ nm for primary and secondary particles, respectively.

Using the statistical models for the numbers of particles of different sizes and surface areas, it is possible to derive descriptors for the size-dependent catalytic activity of both primary and secondary particles by fitting the specific activity data in Figure 2e. On the basis of the work of both Shao et. al[14] and Perez-Alonzo et. al,[24] who carefully studied the effect of particle size on the ORR activity by carefully separating particles with a narrow distribution and DFT calculations, a linear dependence is used to describe the ORR specific activity as a function of particle diameter for Pt nanoparticles ≥2.0 nm (eq S21). It was also assumed that the specific activity of particles with a diameter ≤1 nm was negligible and the specific activity of 1.5 nm particles was ∼2/3 the activity of 2.0 nm particles, also consistent with their work.

The relationship between particle diameter and specific activity of primary particles was determined using eq S22 and the total specific activity data for 2, 3, and 4 deposition cycle Pt/ITO where only primary particles were observed. The combination of the statistical and experimental data found that the specific activity of 2.0 nm primary particles is 0.51 mA/cm^2, and the slope of the specific activity vs diameter for particles above 2.0 nm was 0.88 mA/cm^2·nm. The relationship between particle diameter and specific activity of secondary particles was determined using eq S23 and the total specific activity data for 6, 8, and 10 deposition cycle Pt/ITO where both primary and secondary particles were observed. The specific activity of 2.0 nm secondary particles is 0.25 mA/cm^2, and the slope is calculated as 0.013 mA/cm^2·nm. A detailed explanation for determining the influence of particle size on activity from the statistical and experimental data is provided in the Supporting Information. The activity values and slope clearly show that the preferentially faceted primary particles always have a significantly higher activity, and the margin increases with particle size.

From the statistical description of the particle size distributions and relationships between specific activity and size, eq 4 was used to create a model representation of the specific activity of catalysts as a function of the number of deposition cycles,

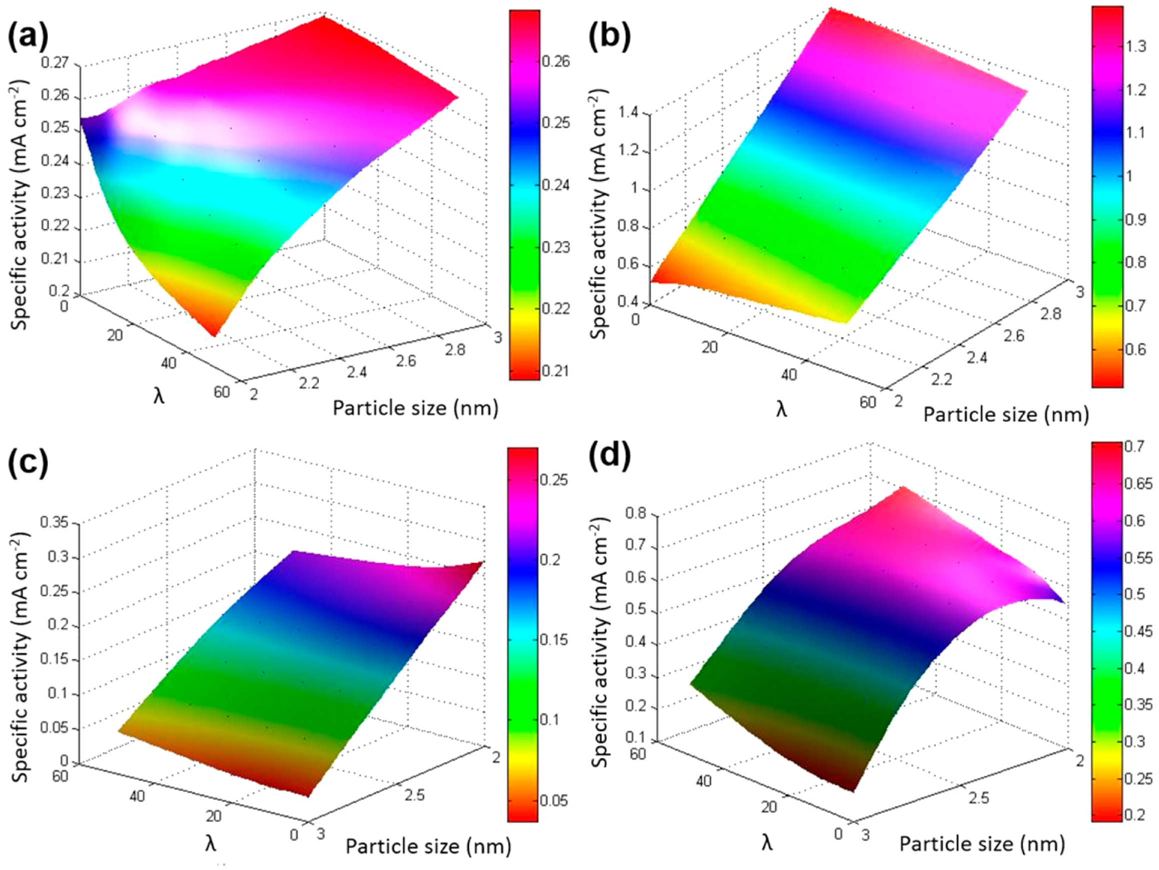

Figure 4. Modeling results of specific activity of (a) Pt/C (b) Pt/ITO; and mass activity of (c) Pt/C (d) Pt/ITO.

$$\mathrm{SA_T} = \theta_\mathrm{P} \sum_{k=5\mathrm{i}}^{40} \mathrm{SA_P}(d)\cdot p(x_\mathrm{P}, \lambda_\mathrm{P}) + \theta_\mathrm{S} \sum_{k=5\mathrm{i}}^{40} \mathrm{SA_S}(d)\cdot p(x_\mathrm{S}, \lambda_\mathrm{S}) \tag{4}$$

where θ_P and θ_S are the portion of surface atoms for primary and secondary particles, respectively (Table S3), and $\mathrm{SA_P}(\mathrm{d})$ and $\mathrm{SA_S}(\mathrm{d})$ are the specific activity of a primary and secondary particles of diameter *d*, respectively.

The model prediction of the specific activity as a function of deposition cycles is shown by the solid line in Figure 2e and nearly perfectly overlays the experimental data. Interestingly, the statistical model predicts an oscillatory behavior for the specific activity with increased Pt loading. The absolute magnitude of the oscillations is not perfectly clear, given their sensitivity to the interpolated particle data (please see the Supporting Information file for more discussion), although the oscillatory behavior predicted by the statistical model was experimentally confirmed by synthesizing a 5 deposition cycle Pt/ITO catalyst, which was not used in the model development (open square in Figure 2e). In the model, the oscillations are a direct consequence of the simultaneous growth of high-activity primary particles and the emergence of lower-activity secondary particles, which cause a leveling off around 0.9 mA/cm^2. The agreement between the experimental and model results for 5 cycles shows the ability of the statistical model not only to describe the existing data but also to be predictive and provide new insight that did not exist in the initial data set.

Another interesting observation from the model is that the secondary particles have an average specific activity of 0.23 mA/cm^2, as calculated from eq 5

$$\sum_{k=5\mathrm{i}}^{40} \mathrm{SA_S}(d)\cdot p(x_\mathrm{S}, \lambda_\mathrm{S}) = 0.23\ \mathrm{mA/cm^2} \tag{5}$$

This value is nearly identical to the value that we previously calculated for Pt/C under the same experimental conditions,[13] which suggests that Pt/ITO secondary particles can be treated as representative of Pt/C when extending the model. This value is less than the value that would be expected for commercial Pt/C catalysts such as 40 wt % Pt/VC HiSPEC 4000 from Johnson Matthey because of its larger average particle size and broader particle size distribution than the Pt/C catalyst prepared in ref 13. However, when we use published data on the average particle size, distribution, and activity of the HiSPEC 4000 catalyst to determine the model parameters,[14,24−26] our model predicts a specific activity of 0.88 ± 0.15 mA/cm^2, consistent with published results for this catalyst (details for this calculation are included in the Supporting Information). This shows specifically how the proposed model can be extended to other ORR catalyst systems and provides a general example for extension to other chemical systems.

The mass activity in Figure 2f was calculated by multiplying the specific activity by the specific ECSA. As expected, the mass activity continuously decreases with increased Pt loading, from 0.66 A/mg$_\mathrm{Pt}$ for 2 deposition cycles to 0.47 A/mg$_\mathrm{Pt}$ for 10 deposition cycles. It is also notable that the mass and specific activities of all of the Pt/ITO catalysts are much higher than commercial Pt/C catalysts, and almost all of them exceed the DOE 2017 targets for mass activity and specific activity.

The excellent ORR activity and ECSA retention suggest that Pt/ITO is ready for immediate implementation in operating

PEMFCs; however, it should be noted that there are some challenges that remain. The synthesis of Pt/ITO by galvanic displacement must be scaled up to produce at least grams per day instead of micrograms per day in the current process. In addition, there is a significant difference between ex situ catalyst performance and the design and construction of an efficient fuel cell electrode. To date, the transition of noncarbon supports to PEMFCs has largely been unsuccessful, and carbon-based supports still offer the highest performance, despite their limitations. One of the reasons for this is that the ink-based electrode fabrication methods that have been used are simply carried over from carbon-based materials, which have properties and behavior vastly different from alternative support candidates, including metal oxides and carbides. Therefore, a considerable effort is still needed to develop processing techniques that explicitly consider the density, hydrophilicity, microstructure, etc. of metal oxide support materials, all of which are vastly different from carbon, to construct high performance PEMFC electrodes.

3.4. Applying the Model as a Catalyst Design Tool.

The predictive ability of the statistical framework described above provides a noncomputationally intense platform to guide future catalyst work for both Pt/C and Pt/ITO ORR electrocatalysts based on secondary and primary particles, respectively. For instance, it is possible to view the relationship between the average particle size and the particle size distribution, exploring a wide parameter space to discover design principles of supported Pt ORR electrocatalysts. Figure 3 showed only a single 2D projection of the relationship between the average particle size and the particle size distribution that was dictated by the synthesis method and conditions. Using the statistical model, it is possible to explore a wider design space to find trends in the specific and mass activities that can guide synthesis.

To explore the influence of the physical characteristics of supported Pt nanoparticles on specific activity and mass activity, the average particle size was parametrically changed in 0.2 nm increments between 2.0 and 3.0 nm, and λ was varied between 0 (perfectly singular particle size) and 50 in increments of 10. This was done for both Pt/ITO and Pt/C. Because they were not observed experimentally, the probability of finding nanoparticles with 1.0 nm > d > 4.0 nm was set equal to zero, and the probability distribution was renormalized. The specific activity was calculated from eq 6,

$$\mathrm{SA} = \sum_{k=10}^{40} \mathrm{SA}(d)\cdot p(x,\lambda) \tag{6}$$

where the index k counts particles between 1.0 and 4.0 nm. Equation 6 differs from eq 5 in that only one type of particle is considered, and the probability distribution is simulated with 0.1 nm accuracy because there is no requirement to compare to experimental data. Pt/ITO is represented by primary particles, and Pt/C is represented by secondary particles.

Figure 4 shows the predictions for both specific and mass activity based on the statistical model. The specific activity increased with particle size for both Pt/ITO and Pt/C, as expected; however, there were significant differences in behavior between these two materials based on particle size distributions. For Pt/C, the specific activity always decreased with increasing λ (widening particle size distribution), shown in Figure 4a. This follows conventional expectation; in fact, it is this "known" trend that has motivated researchers for decades to develop complex synthesis routes to achieve narrow particle size distributions.

For Pt/ITO (Figure 4b), the behavior is more complex. For Pt particle sizes, ≥ 2.8 nm, the same trend as Pt/C is observed. However, at smaller particle sizes, <2.8 nm, the specific activity follows the opposite trend, increasing as the particle size distribution widened. This unexpected trend is a direct result of the very high intrinsic activity of Pt/ITO for the ORR. Alhtough the specific activity is a linear function of particle diameter, the number of surface atoms approximately squares with diameter. The result is that a mixture of 2.0 nm and larger particles has a higher specific activity than a sharp distribution of 2.0 nm particles because there is a threshold particle size where the catalytic enhancement can outpace the increase in surface area. If the slope of activity vs particle size is too small, the threshold particle size falls into a range where structure-sensitive reactions such as the ORR will have very poor activity, <2 nm. Thus, catalysts with smaller slopes, such as Pt/C, will always show decreasing specific activity with widening particle size distribution. On the other hand, as the slope increases, the threshold particle size also increases, eventually entering a range that impacts the behavior of practical catalysts, between 2.6 and 2.8 nm for Pt/ITO. This result provides a significant new insight: if the intrinsic catalyst activity is high enough, conventional wisdom of narrowing the particle size distribution may not apply.

Even more important for operating PEMFCs is the trend in mass activity. The mass activity is best found by multiplying the specific activity by the specific ECSA. Of course, both the specific activity and ECSA are functions of particle diameter. ECSA as a function of particle diameter was determined by fitting a straight line to the 2, 3, and 4 deposition cycle Pt/ITO ECSA data. Mass activity, MA, was calculated as a function of the average particle size and distribution (λ) by

$$\mathrm{MA} = \sum_{k=10}^{40} \mathrm{SA}(d)\cdot \mathrm{ECSA}(d)\cdot p(x,\lambda) \tag{7}$$

For both catalysts, the mass activity decreases with increasing particle size, >2.2 nm, which is expected. Akin to the specific activity, the mass activity of Pt/C (Figure 4c) generally decreases as the particle size distribution widens. Thus, Pt/C has the highest mass activity with the smallest particle size and narrowest particle size distribution. This condition is extremely difficult, if not impossible, to synthesize in the laboratory and would likely be impractical to implement industrially. By contrast, Pt/ITO shows an increase in the mass activity as the particle size distribution widens, regardless of the average particle size (Figure 2d). Thus, the highest mass activity is achieved with 2.2 nm particles and the broadest distribution λ = 50 (standard deviation of 0.7 nm). In addition, looking at the mass activity values (Supporting Information, Table S4) Pt/ITO is considerably less sensitive to particle size distribution than Pt/C. This suggests that existing scalable synthesis methods can achieve high-activity, high-stability Pt/ITO ORR electrocatalysts. There is no need to use complex methods to keep the particle size distribution small; however, care must be taken to maintain the shape and attachment features of Pt/ITO that facilitate the high ORR activity, which to date has been observed only by galvanic displacement.

4. CONCLUSIONS

The properties of Pt/ITO synthesized by galvanic displacement are considerably different from Pt supported on carbon. The synthesis yielded isolated, strongly attached Pt particles at low to intermediate mass loading, which inhibits Ostwald ripening and Pt dissolution. The strong interface bonding is evidenced by continuous lattice fringes from ITO to Pt and preferential {111} facets that yield extraordinarily high specific and mass activities. It is only at very high Pt loadings (>40 wt %) that any appreciable degradation of activity is observed, which correlates with the emergence of secondary particles with weaker substrate interactions. Activity data demonstrate the considerable impact that the support can have on the electrocatalyst size, shape, and dispersion. These physical attributes change as a function of the metal loading and play a key role in dictating catalyst activity and stability. In addition, the excellent ORR activity and ECSA retention of Pt/ITO highlight a new path forward for next-generation ORR catalysts and provide a unique system primed for testing in operational PEMFCs.

The statistical framework developed in this study provides a simple platform to rationalize the influence of particle size and distribution for supported electrocatalysts. From this model, new insights were derived that highlight key differences in the behavior between high-activity and low-activity electrocatalysts. Secondary Pt/ITO particles behave similarly to Pt/C and conform to conventional thinking that narrow particle size distributions lead to the highest specific and mass activities. On the other hand, the higher activity Pt/ITO primary particles benefit from a wider particle size distribution at small sizes and a narrow distribution at larger particle sizes. There are many other applications within heterogeneous catalysis in which activity and particle size data is readily available to the community; this suggests that the framework described herein may be able to provide new insight and have a low activation barrier for implementation over a wide range of materials systems and catalytic platforms.

■ ASSOCIATED CONTENT

Ⓢ Supporting Information

The following file is available free of charge on the ACS Publications website at DOI: 10.1021/cs501556j

> Details for the preparation of the working electrode, Cu deposition, galvanic displacement, experimental details, and Pt loading calculations; specific and mass activity values of Pt/ITO, including the modeling details (PDF)

■ AUTHOR INFORMATION

Corresponding Author

*E-mail: mustain@engr.uconn.edu.

Notes

The authors declare no competing financial interest.

■ ACKNOWLEDGMENTS

This work was funded by the U.S. Department of Energy Office of Basic Energy Sciences, Grant No. DE-FG02-10ER16200. The authors also acknowledge the Institute of Materials Science and the Center for Clean Energy Engineering at the University of Connecticut for free use of the physical characterization tools.

■ REFERENCES

(1) Wagner, F. T.; Lakshmanan, B.; Mathias, M. F. *J. Phys. Chem. Lett.* **2010**, *1*, 2204−2219.

(2) Debe, M. K. *Nature* **2012**, *486*, 43−51.

(3) Gasteiger, H. A.; Marković, N. M. *Science* **2009**, *324*, 48−49.

(4) Marković, N. M.; Ross, P. N., Jr *Surf. Sci. Rep.* **2002**, *45*, 117−229.

(5) Gasteiger, H. A.; Kocha, S. S.; Sompalli, B.; Wagner, F. T. *Appl. Catal., B* **2005**, *56*, 9−35.

(6) Stamenkovic, V. R.; Fowler, B.; Mun, B. S.; Wang, G.; Ross, P. N.; Lucas, C. A.; Marković, N. M. *Science* **2007**, *315*, 493−497.

(7) Song, H.; Kim, F.; Connor, S.; Somorjai, G. A.; Yang, P. *J. Phys. Chem. B* **2004**, *109*, 188−193.

(8) Wang, C.; Daimon, H.; Onodera, T.; Koda, T.; Sun, S. *Angew. Chem., Int. Ed.* **2008**, *47*, 3588−3591.

(9) Nagpal, P.; Lindquist, N. C.; Oh, S.-H.; Norris, D. J. *Science* **2009**, *325*, 594−597.

(10) Nelson, E. C.; Dias, N. L.; Bassett, K. P.; Dunham, S. N.; Verma, V.; Miyake, M.; Wiltzius, P.; Rogers, J. A.; Coleman, J. J.; Li, X.; Braun, P. V. *Nat. Mater.* **2011**, *10*, 676−681.

(11) Lu, J.; Yeo, P. S. E.; Gan, C. K.; Wu, P.; Loh, K. P. *Nat. Nano* **2011**, *6*, 247−252.

(12) Lim, B.; Jiang, M.; Camargo, P. H. C.; Cho, E. C.; Tao, J.; Lu, X.; Zhu, Y.; Xia, Y. *Science* **2009**, *324*, 1302−1305.

(13) Liu, Y.; Mustain, W. E. *J. Am. Chem. Soc.* **2012**, *135*, 530−533.

(14) Shao, M.; Peles, A.; Shoemaker, K. *Nano Lett.* **2011**, *11*, 3714−3719.

(15) Shrestha, S.; Liu, Y.; Mustain, W. E. *Catal. Rev.* **2011**, *53*, 256−336.

(16) Shao-Horn, Y.; Sheng, W.; Chen, S.; Ferreira, P.; Holby, E.; Morgan, D. *Top. Catal.* **2007**, *46*, 285−305.

(17) Pourbaix, M. *Atlas of Electrochemical Equilibria in Aqueous Solutions*; National Association of Corrosion Engineers: Houston, TX, 1974.

(18) Liu, Y.; Mustain, W. E. *Electrochim. Acta* **2014**, *115*, 116−125.

(19) Holby, E. F.; Sheng, W.; Shao-Horn, Y.; Morgan, D. *Energy Environ. Sci.* **2009**, *2*, 865−871.

(20) Ahmadi, T. S.; Wang, Z. L.; Green, T. C.; Henglein, A.; El-Sayed, M. A. *Science* **1996**, *272*, 1924−1925.

(21) Tian, N.; Zhou, Z.-Y.; Sun, S.-G.; Ding, Y.; Wang, Z. L. *Science* **2007**, *316*, 732−735.

(22) Fang, Z.; Patterson, B. R.; Turner, M. E., Jr *Mater. Charact.* **1993**, *31*, 177−182.

(23) Nesselberger, M.; Ashton, S.; Meier, J. C.; Katsounaros, I.; Mayrhofer, K. J. J.; Arenz, M. *J. Am. Chem. Soc.* **2011**, *133*, 17428−17433.

(24) Perez-Alonso, F. J.; Mccarthy, D. N.; Nierhoff, A.; Hernandez-Fernandez, P.; Strebel, C.; Stephens, I. E. L.; Nielsen, J. H.; Chorkendorff, I. *Angew. Chem., Int. Ed.* **2012**, *51*, 4641−4643.

(25) Garsany, Y.; Ge, J.; St-Pierre, J.; Rocheleau, R.; Swider-Lyons, K. E. *J. Electrochem. Soc.* **2014**, *161*, F628−F640.

(26) Garsany, Y.; Ge, J.; St-Pierre, J.; Rocheleau, R.; Swider-Lyons, K. *ECS Trans.* **2013**, *58*, 3−14.